Spin-Printing of Liquid Crystal Polymer into Recyclable and Strong All-Fiber Materials

Gantenbein, Silvan; Mascolo, Chiara; Houriet, Caroline; Zboray, Robert; Neels, Antonia; Masania, Kunal; Studart, André R.

DOI
10.1002/adfm.202104574

Publication date
2021

Document Version
Final published version

Published in
Advanced Functional Materials

ADVANCED FUNCTIONAL MATERIALS
www.afm-journal.de

Spin-Printing of Liquid Crystal Polymer into Recyclable and Strong All-Fiber Materials

Silvan Gantenbein, Chiara Mascolo, Caroline Houriet, Robert Zboray, Antonia Neels, Kunal Masania, and André R. Studart**

Fiber-reinforced polymers are widely used as lightweight materials in aircraft, automobiles, wind turbine blades, and sports products. Despite the beneficial weight reduction achieved in such applications, these composites often suffer from poor recyclability and limited geometries. 3D printing of liquid crystal polymers into complex-shaped all-fiber materials is a promising approach to tackle these issues and thus increase the sustainability of current lightweight structures. Here, we report a spin-printing technology for the manufacturing of recyclable and strong all-fiber lightweight materials. All-fiber architectures are created by combining thick print lines and thin spun fibers as reinforcing elements in bespoke orientations. Through controlled extrusion experiments and theoretical analyses, we systematically study the spinning process and establish criteria for the generation of thin fibers and laminates with unprecedented mechanical properties. The potential of the technology is further illustrated by creating complex structures with unique all-fiber architectures and mechanical performance.

1. Introduction

Fiber-based materials are widespread in biological and synthetic structures. Living organisms produce fibers as mechanical reinforcing elements in a variety of biological materials, from bone and tendons to wood and spider webs.[1–6] The enhanced mechanical properties of fibers have also been exploited in synthetic systems for the fabrication of textiles and composite structures. Depending on the application, synthetic structures can be reinforced with inorganic fibers made out of silica, carbon, silicon carbide and aluminium oxide, or with organic fibers, such as polyethylene, polypropylene and liquid crystal polymers. While the high strength of inorganic fibers results from their small critical defect size,[7,8] the superior mechanical properties of polymer counterparts arise from the strong alignment of macromolecules along the main axis of the fiber.[9]

To achieve molecular alignment, organic fibers are typically produced by spinning processes.[10] In conventional spinning, filaments of the molten polymer or of a gelled polymer solution are subjected to strong extensional flow, followed by fast solidification via cooling or evaporation of the solvent.[11] Alignment of the macromolecules often requires the application of high extensional ratios, which typically range from 10 to 100. These high draw ratios lead to fibers with diameter down to ≈10 µm. After spinning, the polymer fibers can be optionally further treated at temperatures up to 3000 °C to generate carbon fibers for strong lightweight composites.[12] Carbon fiber textiles infiltrated with resins and laid up into laminates of relatively simple geometries is a state-of-the-art composite technology.

The advent of 3D printing technologies has opened the possibility to shape fiber- and particle-reinforced composites into more complex architectures, significantly expanding the design space for lightweight structures.[13–15] Reinforced polymers can be printed by extrusion-based and light-based technologies using resin-coated fibers or resins filled with chopped fibers.[16–19] However, 3D printed composites remain difficult to recycle due to the difficulty in separating its individual components. Fiber-based materials with shape-memory properties or enhanced mechanical performance have also been printed using thermotropic liquid crystal polymers (LCP) as feedstock in extrusion-based processes.[20–23] Molecular alignment in this case is greatly facilitated during printing due to the self-assembly of the polymer into liquid crystal domains.[24] Contrary to polymers reinforced with pre-fabricated fibers, liquid crystal polymer systems can be easily recycled by re-melting and printing the polymer into new print line architectures.[20]

S. Gantenbein, C. Mascolo, K. Masania, A. R. Studart
Complex Materials
Department of Materials
ETH Zürich
Zürich 8093, Switzerland
E-mail: K.Masania@tudelft.nl; andre.studart@mat.ethz.ch

C. Mascolo, C. Houriet, K. Masania
Shaping Matter Lab
Faculty of Aerospace Engineering
Delft University of Technology
Delft 2629 HS, Netherlands

R. Zboray, A. Neels
Empa
Swiss Federal Laboratories for Materials Science and Technology
Dübendorf 8600, Switzerland

The ORCID identification number(s) for the author(s) of this article can be found under https://doi.org/10.1002/adfm.202104574.

DOI: 10.1002/adfm.202104574

However, the print lines generated during 3D printing of LCPs are typically tenfold thicker than the fibers obtained by spinning processes. Since the mechanical properties of LCP fibers were shown to increase significantly for smaller diameters, the implementation of higher extensional rates during extrusion-based printing can potentially lead to the in-situ formation of fibers with performance comparable to those reached via spinning. Previous studies have shown that very thin fibers can be generated by so-called stringing of molten polymer during fused filament fabrication.[25,26] Typically, stringing is considered an undesired artefact of excessive temperature or pressure in the melt. Despite the successful fabrication of fibers, bristles, textiles and hair-like features, the stringing process does not reach the level of fiber diameter control or molecular alignment enabled by conventional spinning, and therefore, has been limited to the creation of aesthetic features during 3D printing.

Here, we propose and study a novel extrusion-based printing technology that enables simultaneous printing and spinning of a molten polymer into strong and recyclable all-fiber materials. The new method, termed spin-printing, is demonstrated using a thermotropic liquid crystal polymer that undergoes strong alignment during printing by fused filament fabrication. To implement the spinning process in an extrusion-based desktop printer, we control the feed rate of the filament such that a small pool of molten polymer is formed at the nozzle tip and is eventually pulled at high draw ratios in air through the rapid lateral motion of the printhead. The effect of filament feed rate on the fiber formation process is systematically studied and later applied for the fabrication of all-fiber laminates and complex structures with enhanced mechanical performance.

2. Results and Discussion

The spin-printing process involves three main operation modes: 1) regular printing through deposition of molten print lines, 2) printing-to-spinning transition, 3) spinning of the fiber in the air (**Figure 1**). The diameter of the print line depends on the nozzle size and the printing height, whereas the diameter of the spun fiber is determined by the feed rate and the translation velocity of the print head. By controlling the feed rate and the velocity of the print head during the printing and spinning modes, it is possible to combine regular print lines (filaments) and spun fibers in a single object using the same feedstock material.

The print line architecture can be designed to generate an object that is preferentially reinforced according to the mechanical loading direction expected in the structural application. For example, in a structure subjected to tensile loading along the longitudinal direction it is desirable to print strong and stiff print lines that follow the stress lines generated in this loading configuration. To keep the structure's integrity and resistance to shear stresses it is also important to provide sufficient strength and modulus in the transverse direction, justifying the deposition of spun fibers orthogonal to the tensile stress lines (Figure 1).

Besides the fiber orientation, the relative fraction of regular print lines and spun fibers is another design parameter that can be easily controlled in the spin-printing process. The strength

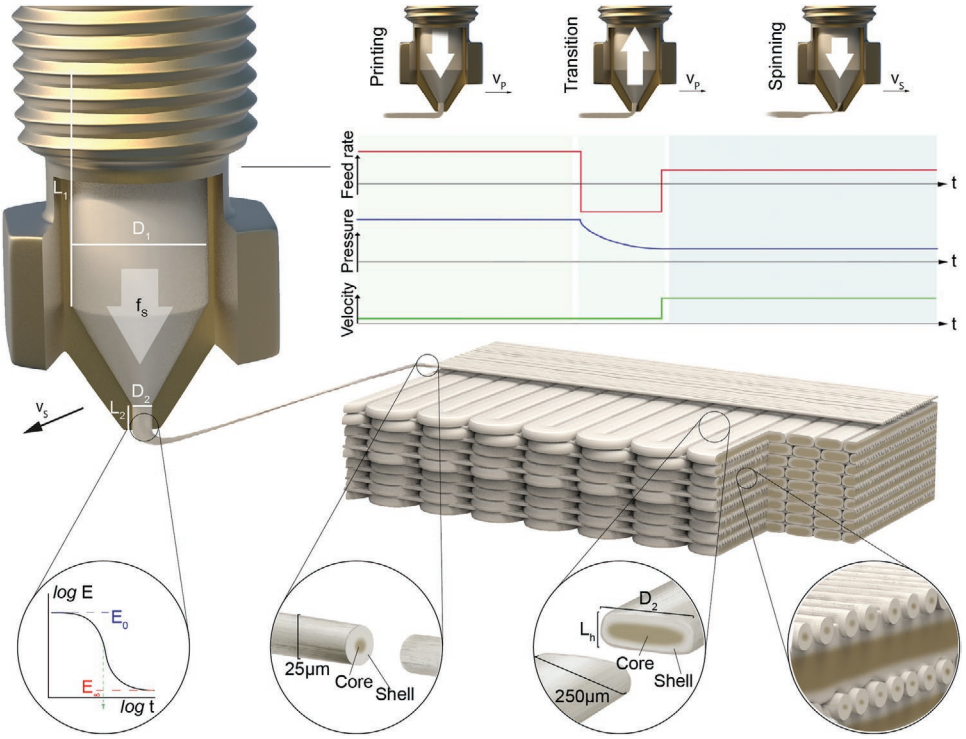

Figure 1. Schematics of the spin-printing technology used for the additive manufacturing of all-fiber materials. Top) Evolution of the applied feed rate, the imposed printhead velocity and the resulting pressure during the main operation modes of printing, transition and spinning. Bottom) Typical viscoelastic response of the molten polymer leading to the extrusion of excess melt (left cartoon) and geometrical features of the spin-printed structure (other cartoons).

and stiffness along a certain direction will depend on the relative volume fraction of fibers printed or spun in that particular orientation. Previous work has shown that the extrusion of liquid crystalline polymers through a 3D printing nozzle leads to print lines with a core-shell architecture, in which the polymer molecules are predominantly aligned within the shell due to rapid cooling of the filament surface. This cooling effect results in a constant shell thickness regardless of the nozzle diameter.[20] Due to their smaller diameter, spun fibers are expected to show a larger fraction of aligned macromolecules and therefore enhanced elastic modulus and mechanical strength compared to regular print lines. Thus, a lower volume fraction of spun fibers is required to reach the same level of strength and stiffness of regular print lines.

To explore this newly accessible design space and define guidelines for the spin-printing of all-fiber structural materials, it is essential to establish a protocol that enables accurate control of the actual volumetric feed rate during the spinning stage of the process. Together with the translational velocity of the print head (v), the volumetric feed rate (f_s) directly affects the diameter of the spun fiber. Using volume conservation arguments, one can show that the diameter of the spun fiber (d_f) is given by the simple relation

$$d_f = \left(\frac{4}{\pi}\frac{f_s}{v}\right)^{1/2} \tag{1}$$

While the printhead velocity is easily controlled by the printer's motor, the actual feed rate of the filament was experimentally found to be different from the nominal feed rate applied. This is due to the viscoelastic nature of the molten polymer, which results in lag of the nozzle pressure. Such effect is particularly noticeable when the feed rate applied needs to be reduced from the high values used for regular printing to the lower target value required to reach a spun fiber of specific diameter (Equation (1)). A simple reduction of the nominal feed rate to the target value leads to initially thick fibers, the diameter of which progressively lowers toward the desired value. This process is known as stringing and was previously exploited to produce hair-like features on printed objects.[25,26] Stringing is caused by the pressure drop across the nozzle needed for extrusion of the material, which does not respond immediately to abrupt changes in the imposed feed rate. For a viscoelastic material, this effect is associated with the slow relaxation of the macromolecules within the molten polymer and oozing of material from the nozzle orifice.

The production of fibers with predictable, uniform diameters requires a modification of the spin-printing protocol to compensate for the excess of molten polymer that would otherwise be extruded due to the high pressure inside the nozzle and the viscoelastic response of the molten polymer. The primary goal of this modification is to ensure that the actual feed rate matches the target value (f_s) throughout the entire spinning regime. To this end, we developed a protocol in which the filament is intentionally retracted from the printing nozzle during the transition regime. Retraction is achieved by applying a retraction feed rate (f_r) to the filament for a certain period of time, t_r. In practice, the feed rate of the filament (F) is often represented in terms of length per unit time. This practical parameter can be converted to the volumetric feed rate (f), by taking into account the cross-sectional area of the printing nozzle: $f = F\pi D_{fil}^2 / 4$, where D_{fil} is the diameter of the feed filament.

To identify the extent of retraction needed to compensate for the delayed pressure decay, we designed a series of experiments in which multiple fibers are sequentially produced through successive spin-printing cycles (**Figure 2**; Figure S1, Supporting Information). In this experiment, the applied retraction feed rate (F_r) is fixed for one specific cycle but increases stepwise between the successive spinning events. The results show that the retraction feed rate can be increased until a critical value is reached, below which the quantity of molten polymer in the print head is insufficient to generate a fiber by spinning (Figure 2b,c). At the critical retraction feed rate, $F_{r,c}$, we expect the excess pressure in the chamber to be fully compensated by the imposed retraction, leading to an actual feed rate at the print head that is equal to the target rate, F_s. Retraction feed rates above $F_{r,c}$ result in stringing, whereas no fiber is formed if $|F_r| > |F_{r,c}|$. By applying a constant retraction feed rate of $F_{r,c}$, we were able to spin fibers with uniform diameter in multiple printing-spinning experiments (Figure 2d). This contrasts with the high variability in fiber diameter observed during stringing, when the nominal feed rate is changed to the F_s value without prior retraction. In this case, the slow decay in pressure over multiple printing events leads to a decreasing diameter over time.

Finding the critical retraction feed rate ($F_{r,c}$) is therefore crucial to spin fibers with predictable diameters. Our experiments reveal that $F_{r,c}$ depends on the print height and on the retraction time, t_r (Figure 2e; Figure S1, Supporting Information). We found that holding the temperature of the nozzle slightly above the melting temperature of the polymer is also crucial to spin fibers with uniform diameters and high mechanical properties (Figure S2, Supporting Information). Moreover, the experiments indicate that the fiber diameter does not depend on the print head velocity as long as the f_s/v ratio is maintained constant, which is in accordance with the prediction of Equation (1) (Figure S3, Supporting Information). We also note that the length of the spin-printed fibers is solely limited by the size of the printer.

To explain the effects of the print height and retraction time on the critical retraction feed rate, we propose a theoretical model that estimates the evolution of the pressure in the molten polymer in the transition phase (Supporting Information). The total pressure is assumed to arise from two major contributions that act in opposite directions. On the one hand, there is the forward pressure applied during the earlier printing phase, which is affected by the relaxation properties of the polymer melt and decays exponentially with a characteristic timescale τ_1. On the other hand, the retraction feed rate imposed in the transition phase leads to a retraction pressure that depends on the viscoelastic properties of the polymer melt through its storage modulus, E_o, and the characteristic timescale, τ_2. By fitting the model to our experimental data, we find that this theoretical analysis leads to reasonable values for the parameters τ_1, τ_2 and E_o (Supporting Information). Because the experimental retraction time ($0.1s < t_r < 0.9s$) is comparable or close to the characteristic timescales obtained from the fitting ($\tau_1 = 2.16s$, $\tau_2 = 0.16s$), we conclude that the critical retraction feed rate is influenced by both the relaxation of the polymer and its reaction to the imposed retraction pressure. By taking the dynamics

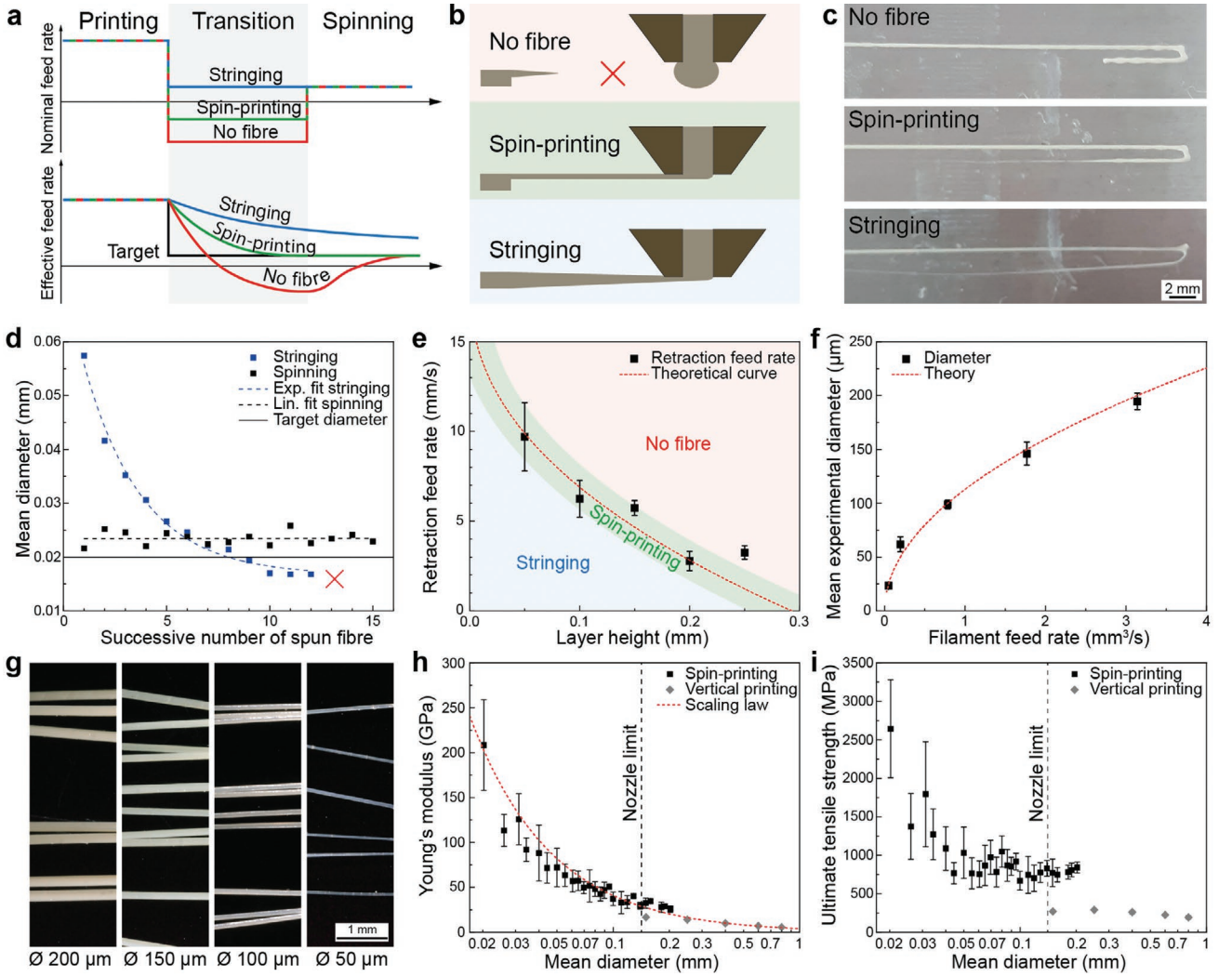

Figure 2. Spinning of strong and stiff fibers through controlled filament feed rate. a–c) Experimental evidence of the critical retraction feed rate required in the transition mode to enable spinning of uniform polymer fibers. The images depict the results of the printing-transition-spinning experiments conducted to identify the critical retraction feed rate, $F_{r,c}$. d) Uniform diameter of fibers produced by spinning compared to the poorly controlled dimensions achieved under stringing conditions. e) Effect of the layer height on the critical retraction feed rate. The dashed line represents a fitting of the theoretical model to the experimental data. f) Dependence of the fiber diameter (d_f) on the volumetric feed rate imposed during spinning. The line indicates predictions from Equation (1). g) Examples of spun fibers of different diameters. h,i) Effect of the fiber diameter on h) the elastic modulus (E) and i) the tensile strength of LCP fibers obtained by spinning compared to previously reported data from vertically extruded print lines.[20] The dashed line corresponds to the scaling relation: $E \approx 1/d_f$.

of the polymer melt into consideration, the model offers a useful tool to predict the critical retraction feed rate needed to spin fibers of uniform diameter and properties (Figure 2e).

Spinning of LCP filaments using the critical retraction feed rates predicted from experiments and theory led to fibers with diameters that closely follow the theoretical predictions from Equation (1) (Figure 2f,g; Movie S1, Supporting Information). By varying the target feed rate between 0.05 and 3.14 $mm^3\ s^{-1}$, fibers with diameters spanning from 23 to 195 μm could be successfully obtained using the proposed spin-printing platform. Importantly, the spinning process allowed us to reach fiber diameters as small as 20 μm, which is not attainable by conventional fused filament fabrication processes. Reducing the diameter to such low values resulted in a remarkable increase in the tensile strength and elastic modulus of individual spun fibers (Figure 2h,i). A tensile strength up to 2.6 GPa and elastic modulus of 208 GPa were achieved for the smallest diameters. These remarkable mechanical properties are comparable to those found for strong and stiff polymer and ceramic fibers.[9,24,27]

The elastic modulus of the fiber was found to increase with the inverse of the fiber diameter ($1/d_f$). In a previous study, we have shown that this dependence arises from the quick cooling of the outer surface of the extruded filament, which leads to a shell of strongly aligned macromolecules around a less oriented inner core.[20] Because the thickness of the cooling-induced shell is constant, the relative fraction of aligned molecules in the fiber increases for smaller diameters. The higher elastic modulus translates into enhanced tensile strengths (Figure 2i).

While the above results suggest that cooling of the extruded fiber controls the structure and properties of the spun fibers,

the high draw ratio imposed during spinning might also contribute to the alignment of the liquid crystals. The draw ratio, λ, is given by

$$\lambda = \frac{D_2^2}{d_f^2} = \frac{\pi D_2^2}{4}\left(\frac{f_s}{v}\right)^{-1} \quad (2)$$

where D_2 is the diameter of the nozzle (Figure 1).

From the reduction in cross-sectional area of the fibers upon spinning (D_2^2 / d_f^2), we find that the draw ratio applied in our experiments reaches up to 200, which is comparable to the ratios used for the spinning of ultra-high-molecular-weight (UHMW) polyethylene fibers. As an example, to achieve a draw ratio of 200, the printhead velocity (v) was fixed at 100 mm s^{-1} while imposing a target feed rate (f_s) of 0.06 mm^3 s^{-1}. Such high draw ratios are expected to be sufficient to also align UHMW polyethylene fibers using the proposed spin-printing platform.

The ultrahigh strength and elastic modulus of the spun-printed fibers enables the design and fabrication of bulk, recyclable laminates with enhanced mechanical properties. To explore this potential, we fabricate bulk specimens with a laminate architecture combining thick print lines and thin spin-printed fibers with orthogonal orientations (**Figure 3**). The thick print lines constitute more than 90% of the laminate and are used to provide high strength and stiffness along one specific direction. Because this longitudinal orientation of thick print lines reduces the transverse mechanical properties of the laminate, thin fibers are spin-printed orthogonally to enhance the strength and elastic modulus of the structure along the weaker direction.

Bulk laminates with orthogonal reinforcement were created by printing 0.25 mm wide print lines along one direction and spin-printing up to 8 vol% of 25–30 µm diameter fibers in the transverse orientation within each print layer (Figure 3a). While

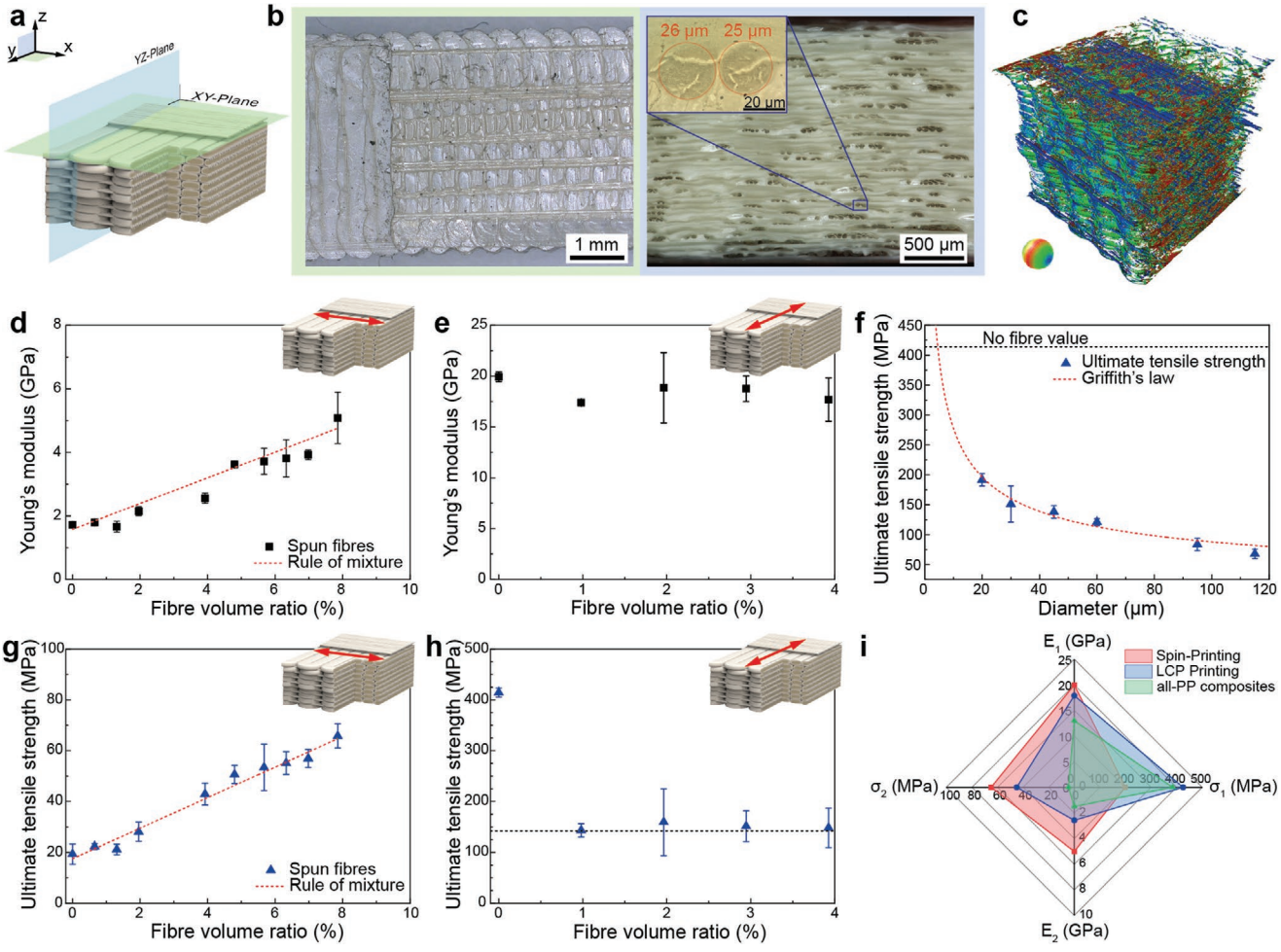

Figure 3. Structure and mechanical properties of spin-printed LCP laminates. a,b) Optical microscopy images of laminates consisting of thicker print lines and thinner fibers arranged orthogonally to each other. c) P 3D representation of microCT measurements indicating qualitatively the fiber orientation according to the colour sphere. d,e) Elastic modulus and g,h) tensile strength of laminates with increasing volume fraction of fibers obtained under different tensile loading configurations. Tensile stresses are applied either perpendicular (transverse, (d,g)) or parallel (longitudinal, (e,h)) to the thicker print lines as indicated by the red arrows in the cartoons. f) Effect of the diameter of the fiber on the tensile strength of laminates tested in the longitudinal configuration. The dashed line shows the theoretical prediction based on Griffith's law. i) Elastic modulus (E) and tensile strength (σ) of spin-printed LCP laminates along the longitudinal and transverse directions compared to the mechanical performance of printed LCP[20] and all-poly(propylene) composites.[28]

the spin-printing process increases the overall printing time, the high spinning speed applied reduces significantly this time overhead. A typical 10cm-long fiber spun at a printhead velocity of 100 mm s^{-1} is produced in ≈1 s. For a laminate containing 8% fibers in longitudinal direction, 36 fibers are deposited per layer. Spin-printing these fibers on a typical 40-layer laminate increases the print time by 24 min, which is 70% longer compared to specimens without spun fibers. Notably, because no matrix material is required as a binding phase in between fibers, the laminate can be fully recycled by melting and re-printing the polymer feedstock into new fiber architectures that meet the mechanical demands of the desired application (Figure S4, Supporting Information).

Optical microscopy images and microcomputed tomography of the bulk laminate reveal that the spin-printed fibers form bundles of 2–8 individual thin fibers between the thicker orthogonal printed layers (Figure 3a–c; Figure S5 and Movie S2, Supporting Information). This bundling effect is caused by the lateral displacement of the already spun fibers during the deposition of the next layer of orthogonal print lines (see Movie S1, Supporting Information). Lateral displacement happens when the actual spun fibers are longer than the programmed spinning length, which most likely arises from the negative thermal expansion coefficient of oriented LCPs. This effect causes the spun fibers to elongate during cooling and thus deviate from their optimal straight configuration. For the spinning length of 60 mm used in these experiments, a fiber elongation of only 0.0012 % is enough to result in a lateral displacement of 0.15 mm, which is the distance separating individual spin-printed fibers. Such lateral displacement and bundling effect lead to suboptimal fiber orientation and structural reinforcement.

To evaluate the effect of the orthogonal spin-printed fibers on the mechanical properties of the bulk laminates, we measured the fracture strength and elastic modulus of specimens subjected to tensile loading along the longitudinal (0°) and transverse directions (90°). The results of the mechanical tests show that the incorporation of 7.9 vol% of spun fibers enhances by a factor of, respectively, 3.4 and 3 the fracture strength and the elastic modulus of the laminate along the weaker 90° orientation (Figure 3d,g). The observed reinforcement is in good agreement with theoretical predictions based on a simple rule-of-mixtures model (Supporting Information). Moreover, experiments with other laminate architectures reveal that spun fibers provide more effective transverse reinforcement compared to orthogonal print lines or printed layers at the same volume fraction (Figure S6, Supporting Information). While the elastic modulus of these structures is unaffected, the strength of the laminates decreases with increasing fiber content. This indicates that the fibers mainly act as defects in such architectures. Interestingly, the deposition of thin spun fibers along the same longitudinal direction as the printed lines was found to be an ineffective reinforcement approach, possibly again due to the lateral displacement and bundling of the spun fibers in this laminate architecture (Figure S7, Supporting Information).

The use of transverse spun fibers to reinforce the weaker orientation of the laminate was found to affect the mechanical strength of the specimens along the stronger longitudinal direction (Figure 3e,h). While the elastic modulus of the laminate remains unaltered at the high level of around 19 GPa, the strength of the laminate decreases from 414 to 143 MPa upon the incorporation of 1 vol% of transverse spun fibers. Importantly, the mechanical strength of the laminate remains at around 150 MPa if the volume content of spun fibers is further increased to 3.9 vol%. The observed drop in mechanical strength might be explained by the fact that the transverse spun fibers act as defects that concentrate stress and thereby provide crack initiation sites for fracture of the mechanically loaded laminate (Figure S8, Supporting Information). To test this hypothesis, we measured the mechanical strength of laminates containing transverse spun fibers with different diameters, which should therefore lead to distinct critical defect sizes, c. According to Griffith,[8] the fracture strength of a brittle material scales with $1/c^{1/2}$. By fitting this simple relation to our experimental data, we find that the strength of the laminates can be reasonably described using the scaling proposed by Griffith (Figure 3f). This supports the above interpretation that the transverse spun fibers reduce the longitudinal tensile strength of the laminate by concentrating stresses locally and thus initiating the propagation of cracks.

To put the measured mechanical properties in perspective, we compare the strength and elastic modulus of our reinforced laminates to those of other all-fiber recyclable materials tested in transverse and longitudinal orientations (Figure 3i).[28] The comparison with longitudinally printed LCP shows that the reinforcement of bulk laminates with spun fibers oriented at 90° enhances significantly the transverse strength and elastic modulus of the structure at the cost of a lower longitudinal strength. This trend is more pronounced when the reinforced LCP laminates are compared with all poly(propylene) structures produced by hot compaction of co-extruded tapes. In this case, the transverse strength and elastic modulus of the reinforced LCPs is, respectively, 14- and 3-fold higher than that of the poly(propylene) counterpart. Such transverse reinforcement is accompanied by a 55 % reduction in longitudinal strength. Overall, our experiments indicate that spin-printed fibers can be effectively used to generate reinforced bulk laminates with mechanical properties that are less orientation dependent and therefore suitable for more complex mechanical loading conditions.

In addition to reinforced bulk laminates, the ability to spin-print fibers with high mechanical properties can also be exploited to fabricate complex fiber-based structures that are not accessible using conventional manufacturing approaches (**Figure 4**). We illustrate this potential by spin-printing a range of objects with fiber architectures that are deliberately designed to leverage the high strength and stiffness of spin-printed fibers under tensile loading (Figure 4a). In these examples, spin-printed fibers are positioned and oriented such that they carry tensile stresses arising from mechanical loading, thereby improving the load-bearing capacity of the structure.

Using a simple ring geometry, we quantify the reinforcing effect of such fibers by experimentally measuring the load-bearing capacity and mechanical stiffness of bespoken structures under compression (Figure 4b–d; Movie S3, Supporting Information). Motivated by the periodic nodes that prevent

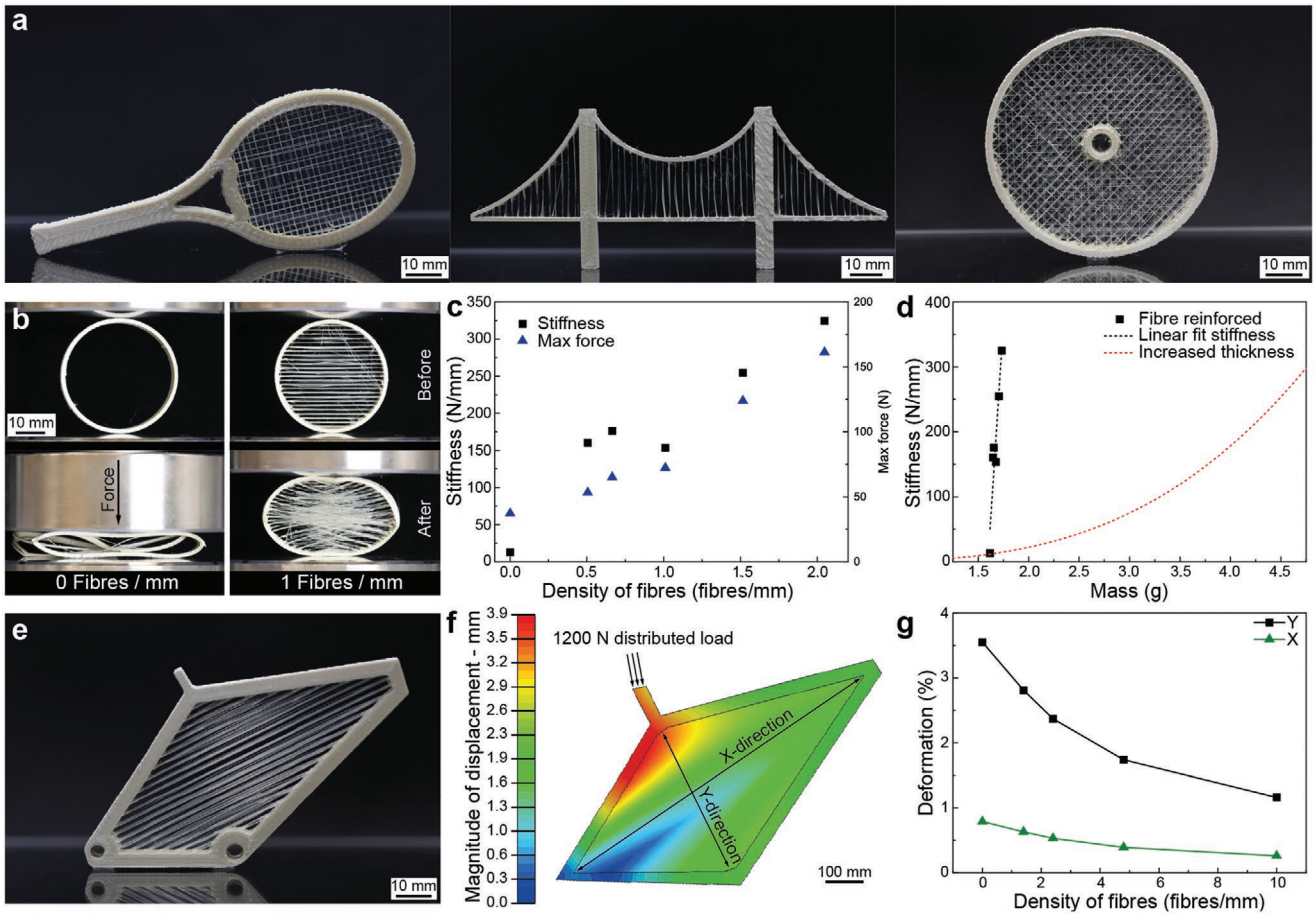

Figure 4. Complex structure and mechanical behaviour of LCP objects generated by the spin-printing technology. a) Examples of complex structures displaying spin-printed fibers that are designed to carry tensile stresses upon specific mechanical loading conditions. b) Snapshots of compression tests on LCP rings reinforced by spanning fibers (right) in comparison to a reference non-reinforced specimen (left). c) Effect of the density of fibers on the stiffness and load-bearing capacity of the ring-shaped object under compression. d) Variation of mechanical stiffness with mass of the ring for specimens reinforced by spanning fibers as compared to a reference object with increasing wall thickness. e) Miniaturized bicycle frame design reinforced by spanning fibers. f) Finite element analysis of a mechanically loaded bicycle frame, depicting the strain distribution when reinforced by 10 fibers per mm in *X*-direction. g) Effect of the density of fibers on the simulated deformation of the bicycle frame along distinct directions.

cross-sectional flattening in bamboo, we prepared structures that replicate their internal reinforced architecture. In this case, the structure is reinforced by spin-printing fibers that span between the opposite sides of the ring. To effectively reinforce the structure, the spanning fibers are oriented perpendicular to the compression direction. Experiments on specimens with different levels of reinforcement reveal that the mechanical stiffness and load-bearing capacity of the ring increases significantly with the density of fibers spanning across the structure (Figure 4b,c). The beneficial effect of the reinforcing fibers is most evident, if we compare the mass of additional polymer needed to increase the ring stiffness either by increasing its thickness or by incorporating spanning fibers. The comparison shows that the structure reinforced with spanning fibers requires 3-times less mass than a thickened ring to increase by 25-fold the mechanical stiffness of the initial object (Figure 4d).

This spanning-fiber reinforcement concept can also be extended to more complex geometries. We demonstrate this by spin-printing a miniaturized bicycle frame, in which the load-bearing seat tube element is removed from the structure and replaced by fibers spanning perpendicular to the load direction (Figure 4e). To evaluate the effect of the spanning fibers on the mechanical performance of the bike frame, we performed finite element analysis of the real-life structure when subjected to a compressive load that emulates the weight of the biker. In this analysis, the spanning fibers are represented by wires with well-defined mechanical properties and orientation relative to the bike frame. The simulation shows that the vertical and horizontal deformations of the structure under the compressive load decrease by as much as 3 times, respectively, upon the incorporation of fibers spanning perpendicular to the loading direction. This approach demonstrates the possibility of tuning the stiffness of a structure through geometry and hierarchical damping,[20] thereby supressing the need for the addition of suspension on the frame. This stiffening concept is potentially applicable to structures with other geometries, as long as the fiber architecture is designed such that the spanning fibers are subjected to tensile loading.

3. Conclusion

In summary, the proposed spin-printing technology enables shaping of thermotropic liquid crystal polymers into strong, recyclable complex objects with tunable direction-specific mechanical properties. In-situ spinning of fibers with diameters down to 20 µm is possible by closely controlling the actual feed rate of the feed filament during the extrusion process. Because of the viscoelastic nature of the molten polymer, the feed filament needs to be retracted at a critical retraction feed rate prior to spinning in order to ensure the formation of thin fibers with uniform diameter. With a diameter tenfold smaller compared to print lines, the spun fibers reach remarkable tensile modulus and strength of 208 and 2.6 GPa, respectively. The ability to deposit such thin fibers on top of print lines during the manufacturing process allows for the on-the-fly reinforcement of laminates and complex structures in deliberate directions. This feature can be exploited to design and fabricate fiber architectures that match the mechanical loading conditions of the application of interest. Since the printed objects are fully recyclable, multi-axis fiber architectures can be re-programmed multiple times to fulfil distinct mechanical demands. Extending this spin-printing concept to liquid crystal elastomers and other thermoplastic polymers should open new manufacturing opportunities for shape-changing materials or all-fiber recyclable structures.

4. Experimental Section

Preparation of LCP Filament: The feed filaments used as feedstock in the desktop printer were produced by extrusion of the commercially available thermotropic liquid crystal polymer Vectra A 950 (Celanese). Vectra A950 pellets were dried for 24 h at 150 °C before extrusion. A single-screw extruder (Teach-Line E20 T, Collin) was used to produce the LCP filaments at 60 rpm. The three barrel zones of the extruder were heated to 270, 295, and 295 °C, while the nozzle temperature was set to 280 °C. After extrusion, the filament was cooled in a water bath and wound on a modified flat film line (Teach-Line CR72 T, Collin). To produce filaments with a diameter of 1.75mm, the rotational speeds of the extruder's screw and the winder's were fine-tuned during the extrusion process.

Fused Filament Fabrication (FFF): In this work, a commercial desktop FFF printer (Ultimaker 2+, Ultimaker) was modified with a direct drive extruder (E3D Hemera) to achieve temperatures up to 400 °C. Before printing, a thin layer of poly(vinyl alcohol)-based adhesive (Dimafix Pen) was laid on the borosilicate glass build plate to improve LCP adhesion. The build plate was heated to 100 °C during this pre-coating process. Unless otherwise stated, the samples were printed with a nozzle temperature of 295 °C at a print-head speed of 35 mm s^{-1} without any active cooling. A higher print-head velocity of 100 mm s^{-1} was used during spinning.

Print paths (G-codes) were generated with a custom slicer using Grasshopper for Rhinoceros (McNeel). The approach used for the fabrication of uniform fibers involves a complete cycle of multiple printing-spinning-printing steps separated by transition phases. Firstly, an anchor is printed at a speed of 35 mm s^{-1}, a set layer height of typically 0.05 mm and width equal to the nozzle diameter. This is followed by a transition phase, in which the feed filament is retracted at a certain retraction feed rate (F_s) over a set period of time. Then, the print-head is vertically lifted by ≈0.1 mm and translated laterally at a speed of 100 mm s^{-1} to enabling fiber spinning. Afterward, printing proceeds with a second transition phase, in which the feed filament is pushed forward at the same feed rate (F_s) for the same time and printing conditions applied in the first transition phase. Finally, a second anchor is printed to complete the spin-printing cycle.

Mechanical Testing of Fibers: Tensile tests were carried out to characterise the mechanical properties of spun fibers. Fibers with different diameters were produced by varying the nozzle diameter, the nozzle temperature, the distance to the build-plate surface (layer height) and retraction feed rates. Before tensile tests, samples were glued (3M Scotch-Weld Epoxy Adhesive DP100) onto paper frames to ensure a constant gauge length of 20 mm. Fiber samples were tested in tension at a rate of 2 mm min^{-1} using a universal testing machine with a 1 kN capacity load cell (AGS-X, Shimadzu). Five samples were tested for each fiber diameter. The diameter of the fibers was determined before testing with a digital microscope (VHX-6000, Keyence). Data analysis was performed using a custom MATLAB script.

Mechanical Testing of Printed Laminates Reinforced with Thin Spun Fibers: Tensile tests were performed on printed laminates containing thin spun fibers integrated between each layer. To ensure good adhesion between the thin fibers and the underlying layer, anchors were printed before and after spinning. Two sets of specimens were spin-printed to study the mechanical properties of the fiber-reinforced laminates along the longitudinal and transverse directions. In the first set, specimens were prepared by printing print lines and fibers oriented at an angle of, respectively, 0° and 90° relative to the loading direction (0/90 samples). The second set of samples consisted of thick print lines at an angle of 90° and fibers at an angle of 0° with respect to the testing direction (90/0 samples). For sake of comparison, tensile test samples were also printed with both print lines and fibers oriented at 0° with respect to the testing direction (0/0 samples). For all these specimens, the volume fraction of thin spun fibers in the laminate was systematically varied by changing the number of fibers deposited per layer.

To evaluate the advantage of reinforcing laminates with thin spun fibers orthogonal to the print lines, two additional types of specimens were produced. In these samples, the orthogonal thin fibers were replaced either by isolated print lines or by full printed layers (Figure S6, Supporting Information). The volume fraction of transverse reinforcement was kept constant for all the specimens.

Five samples were tested for each batch using a universal testing machine with a 20 kN capacity load cell (Z020, Zwick). All the specimens had a nominal width of 4.5mm, a length of 110 mm and a thickness of 2 mm. Glass fibers tabs were glued to the sample ends (3M Scotch-Weld Epoxy Adhesive DP460) to support the samples in the clamping region, resulting in a gauge length of 60 mm. Data analysis was performed using a custom MATLAB script.

Mechanical Testing of Fiber-Reinforced Ring Structures: To study the effect of spanning fibers on the mechanical performance of ring-shaped structures (Figure 4b), samples with densities of parallel spanning fibers varying from 0 to 77 fibers per layer were spin-printed. The rings display an outside diameter of 40 mm, a wall thickness of 1.2 mm and a height of 7.9 mm.

Lateral compression tests were performed at constant rate of 2 mm min^{-1} using a universal testing machine with a 1kN capacity load cell (AGS-X, Shimadzu). Specimens were tested laterally and oriented so as to align the spanning fibers parallel to the compression plates. This configuration ensured that the spanning fibers were loaded in tension upon compression.

In order to assess the benefit of incorporating spanning fibers into the ring structure, the stiffness of the fiber-reinforced rings was compared to that of fiber-free counterparts of equivalent stiffness through increased thickness. For fiber-reinforced rings, the stiffness was determined from the first derivative of the elastic region of the experimentally obtained load-deflection curves. To estimate the thickness required for the fiber-free ring to reach a stiffness equivalent to that of the fiber-reinforced structures, the following relation was used[29]

$$S = \frac{1}{24\pi^2\left(\pi^2-8\right)}\frac{E}{\beta l^2 r_o^6 \rho^3} m^3 \quad (3)$$

where S is the mechanical stiffness of the structure defined as the slope of the load-deflection curve in the elastic regime, l is the length of the ring, r_0 is the outer radius of the ring, E is the elastic modulus of the material, ρ is the specific gravity of the material, β is constant equal to 1 for plane stress condition, and m is the mass of the ring.

Microscopic Analysis: Optical images were taken with a digital microscope (VHX-6000, Keyence) to observe the transverse and longitudinal sections of non-tested tensile specimens. Before imaging, the samples were cut, embedded in epoxy, and polished. Polishing was conducted using SiC paper with decreasing roughness (increasing grit size, #) in the following sequence and duration: #500 for 1.5 min, #1000 for 1.16 min, #2000 for 1.5 min, and finally two steps with #4000 for 2 min. Between each step, the specimens were cleaned under running water and dried with compressed air.

Micro Computed Tomography Analysis: To visualize the thin fibers embedded in the printed laminates, micro CT analysis was carried out by the Centre for X-ray Analytics at Empa (Switzerland). CT images were obtained for both 90/0 and 0/0 samples with dimensions $2 \times 2 \times 100$ mm using the RX Solutions EasyTom XL Ultra 230-16 system (RxSolutions SAS, Chavanod, France). The scanner features a Hamamatsu nano-focus X-ray tube with transmission target and was operated at an acceleration voltage of 75 kV and tube current of 50 µA. The detector used was a CCD camera with 2016×1344 Pixel (18 µm pixel size) and voxel size was 1.5 µm for CT encompassing around 2 mm of height in the center of the sample. The images were acquired at 2.0 s exposure and averaging 3 frames per projection taking 1568 projections.

Finite Element Analysis of Fiber-Reinforced Bicycle Frame: To study the influence of thin fibers spanning across a bike frame, we performed numerical simulations on ABAQUS (Abaqus FEA, Dassault Systèmes Simulia). The frame geometry consisted of a classic bike frame, with the central seat tube replaced with a varying number of thin fibers spanning across the structure perpendicular to the loading direction. The bike frame was sketched in Abaqus CAE as a 2D planar shell in a 3D domain. To represent the spanning fibers, wires were connected to the inner edge of the bike frame. Due to the large density of wires (up to 1 wire/0.1 mm) the inner edges were automatically seeded for the wire endpoints using Python in a modified journal (.JNL) file read by ABAQUS. Using the same method, the wires were then created on either side of these points to be parallel to one another. Material properties were assigned to both the set of wires and the planar bike frame. The wires were set to be made of an isotropic material with a Young's modulus of 80GPa, a null Poisson's ratio and zero compressive modulus. The frame was considered as a laminate with mechanical properties previously reported for printed LCP.[20] To estimate these mechanical properties, we assume that the shear modulus in transverse directions is equal to the in-plane shear modulus. The laminate was composed of 200 layers, each with a thickness of 0.05mm and oriented parallel to the longitudinal axis of each individual bar of the bike frame. The mesh was built from quad-dominated element shapes (8-node doubly curved thick shell for the laminate and 2-nodes linear 3D trusses for the wires). In the presence of wires, the meshing is refined so that one common node exists at the wire/frame interface. To evaluate the effect of the spanning fibers on the deformation of the structure, a load of 1200 N was evenly distributed along the top of the seat post top, pointing downward (Figure 4f). The magnitude and direction of the applied load were chosen to simulate the weight of a cyclist with a margin of safety for impacts. The frame is constrained to prevent displacements in the Z direction and thus study the effect of the wires on the bike deformation within the XY-plane. To simulate both the back and front wheels, the bottom left angle was pinned in X,Y,Z displacements, while the top right point was pinned in a local X coordinate to prevent the bike frame from rotating under the cyclist load. A static, general linear analysis was performed while taking into account the boundary conditions described above. The X–Y displacements are node displacements of the frame measured with respect to a XY local coordinate axis, where Y was aligned with the wire orientation.

Supporting Information

Supporting Information is available from the Wiley Online Library or from the author.

Acknowledgements

The authors thank the Swiss Competence Center for Energy Research (SCCER – Capacity Area A3: Minimization of energy demand) and the Swiss National Science Foundation (SNSF consolidator grant BSCGIO_157696) for financially supporting this research. The research also benefitted from support from the Swiss National Science Foundation within the framework of the National Center of Competence in Research for Bio-Inspired Materials. Finally, the authors would also like to thank Prof. Theo Tervoort (ETH Zurich) for the helpful discussions.

Open access funding provided by Eidgenossische Technische Hochschule Zurich.

Conflict of Interest

S.G., K.M., and A.S. are co-founders of the company NematX, which develops 3D printed high-performance polymers.

Author Contributions

S.G. and and C.M. contributed equally to this work. S.G. conceived the idea together with K.M., C.M., and A.R.S. S.G. and C.M. carried out the majority of experimental work. C.H. performed the FE analysis, whereas R.Z. and A.N. performed the µ-CT measurements. S.G., C.M., K.M., and A.R.S. analyzed and interpreted the data. S.G., C.M., C.H., and A.R.S. wrote the paper, which was thoroughly revised by K.M., R.Z., and A.N.

Data Availability Statement

The data that support the findings of this study are available from the corresponding author upon reasonable request.

Keywords

3D printing, additive manufacturing, fused filament fabrication, polymer technology, structural materials

Received: May 14, 2021
Revised: September 3, 2021
Published online:

[1] S. W. Cranford, A. Tarakanova, N. M. Pugno, M. J. Buehler, *Nature* **2012**, *482*, 72.
[2] U. G. K. Wegst, *J. Mech. Behav. Biomed. Mater.* **2011**, *4*, 744.
[3] P. Kannus, in *Structure of the Tendon Connective Tissue*, Copenhagen, Denmark **1999**, pp. 312–320.
[4] S. Weiner, H. D. Wagner, *Annu. Rev. Mater. Sci.* **1998**, *28*, 271.
[5] F. Vollrath, D. P. Knight, *Nature* **2001**, *410*, 541.
[6] U. G. K. Wegst, H. Bai, E. Saiz, A. P. Tomsia, R. O. Ritchie, *Nat. Mater.* **2015**, *14*, 23.
[7] H. J. Gao, B. H. Ji, I. L. Jager, E. Arzt, P. Fratzl, *Proc. Natl. Acad. Sci. USA* **2003**, *100*, 5597.

[8] A. A. Griffith, *Philos. Trans. R. Soc.* **1920**, *A221*, 163.
[9] J. Lefevre, K. Feldman, J. Giesbrecht, P. Smith, T. A. Tervoort, H. E. H. Meijer, *J. Polym. Sci., Part B: Polym. Phys.* **2012**, *50*, 1713.
[10] T. Peijs, in *Comprehensive Composite Materials II* (Eds: P. W. R. Beaumont, C. H. Zweben), Elsevier, Oxford **2018**, pp. 86–126.
[11] P. Smith, P. J. Lemstra, *J. Mater. Sci.* **1980**, *15*, 505.
[12] X. Huang, *Materials* **2009**, *2*, 2369.
[13] X. Wang, M. Jiang, Z. Zhou, J. Gou, D. Hui, *Composites, Part B* **2017**, *110*, 442.
[14] D. Kokkinis, M. Schaffner, A. R. Studart, *Nat. Commun.* **2015**, *6*, 8643.
[15] G. Siqueira, D. Kokkinis, R. Libanori, M. K. Hausmann, A. S. Gladman, A. Neels, P. Tingaut, T. Zimmermann, J. A. Lewis, A. R. Studart, *Adv. Funct. Mater.* **2017**, *27*, 1604619.
[16] B. G. Compton, J. A. Lewis, *Adv. Mater.* **2014**, *26*, 5930.
[17] J. P. Lewicki, J. N. Rodriguez, C. Zhu, M. A. Worsley, A. S. Wu, Y. Kanarska, J. D. Horn, E. B. Duoss, J. M. Ortega, W. Elmer, R. Hensleigh, R. A. Fellini, M. J. King, *Sci. Rep.* **2017**, *7*, 43401.
[18] F. V. D. Klift, Y. Koga, A. Todoroki, M. Ueda, Y. Hirano, R. Matsuzaki, *Open J. Compos. Mater.* **2016**, *06*, 10.
[19] T. Hofstätter, D. B. Pedersen, G. Tosello, H. N. Hansen, *J. Reinf. Plast. Compos.* **2017**, *36*, 1061.
[20] S. Gantenbein, K. Masania, W. Woigk, J. P. W. Sesseg, T. A. Tervoort, A. R. Studart, *Nature* **2018**, *561*, 226.
[21] A. Kotikian, R. L. Truby, J. W. Boley, T. J. White, J. A. Lewis, *Adv. Mater.* **2018**, *30*, 1706164.
[22] M. López-Valdeolivas, D. Liu, D. J. Broer, C. Sánchez-Somolinos, *Macromol. Rapid Commun.* **2018**, *39*, 1700710.
[23] C. P. Ambulo, J. J. Burroughs, J. M. Boothby, H. Kim, M. R. Shankar, T. H. Ware, *ACS Appl. Mater. Interfaces* **2017**, *9*, 37332.
[24] R. Schaller, T. Peijs, T. A. Tervoort, *Composites, Part A* **2016**, *81*, 296.
[25] G. Laput, X. A. Chen, C. Harrison, in *Proc. of the 28th Annual ACM Symp. on User Interface Software and Technology*, Association for Computing Machinery, Charlotte, NC, USA **2015**, pp. 593.
[26] H. Takahashi, J. Kim, in *Proc. of the 32nd Annual ACM Symp. on User Interface Software and Technology*, Association for Computing Machinery, New Orleans, LA, USA **2019**, pp. 43–51.
[27] L. C. Sawyer, M. Jamieson, D. Brikowski, M. I. Haider, R. T. Chen, *J. Am. Ceram. Soc.* **1987**, *70*, 798.
[28] B. Alcock, N. O. Cabrera, N. M. Barkoula, J. Loos, T. Peijs, *Composites, Part A* **2006**, *37*, 716.
[29] G. Rathnaweera, Y. Durandet, D. Ruan, S. Kinoshita, *Int. J. Prot. Struct.* **2011**, *2*, 465.